



Contents lists available at ScienceDirect

International Biodeterioration & Biodegradation

journal homepage: www.elsevier.com/locate/ibiod

Sorption behavior of Cr(VI) on pineapple-peel-derived biochar and the influence of coexisting pyrene

Chuanhua Wang^{a, b}, Lingfeng Gu^a, Xiaoyan Liu^{a, *}, Xinying Zhang^a, Liya Cao^a, Xiaoxin Hu^a^a College of Environment and Chemical Engineering, Shanghai University, Shanghai 200444, China^b College of Life and Environment Science, Wenzhou University, Wenzhou, Zhejiang 325035, China

ARTICLE INFO

Article history:

Received 12 December 2015

Received in revised form

16 April 2016

Accepted 23 April 2016

Available online 2 May 2016

Keywords:

Hexavalent chromium

Biochar

Sorption behavior

Pyrene

Coexistence

ABSTRACT

The influence of pyrolytic temperatures and of the properties of pineapple-peel-derived biochar (PABC) on Cr(VI) sorption behavior with and without pyrene was investigated. The structural characteristics of PABC were analyzed by scanning electron microscopy (SEM), and the surface groups of PABC were analyzed before and after Cr(VI) sorption, using Fourier transform infrared spectroscopy (FTIR). The results indicate that the characteristics of PABC depend on the pyrolytic temperature, and the adsorption isotherms fit well with the Freundlich equation. The greatest sorption capacity, 7.44 mg g⁻¹, occurred with PABC pyrolyzed at 750 °C for 2 h. In addition, the slow sorption kinetics fit well with second-order reaction kinetics. When pyrene coexisted in the solution, the adsorption of Cr(VI) was inhibited because of the inner complex between the hydroxyl groups on PABC and pyrene flushbonading the H bond with Cr(VI). There were no significant changes in the functional groups of the biochar surface between the two sides of the adsorption equilibrium, which demonstrates the slight contribution of organic matter in chromium adsorption. PABC has the potential to remove Cr(VI), but the presence of pyrene can inhibit Cr(VI) adsorption.

© 2016 Elsevier Ltd. All rights reserved.

1. Introduction

Chromium appears in nature mainly in trivalent and hexavalent forms (Mohan and Pittman Jr., 2006; Pan et al., 2014; Yu and Gu, 2008). The wide use of chromium in industry is its main anthropogenic source (Tytlak et al., 2015; Yu et al., 2007). Chromium contamination in surface water, soil, or groundwater has been detected at and around a wide variety of industrial sites. Chromium contaminants have led to adverse effects on the cell membranes of living organisms and affect human health by eventually passing through the food chain.

The trivalent and hexavalent states of chromium have different properties such as bioavailability, mobility, and toxicity. Cr(VI) is more dangerous to public health and to the ecosystem than Cr(III) because of its higher toxicity, mutagenicity, carcinogenicity, teratogenicity, and mobility (Yu et al., 2008). Unlike Cr(VI), Cr(III) has a

low solubility and tends to stick to soil particles in normal conditions (Hsu et al., 2009). Hexavalent chromium compounds are approximately 1000 times more mutagenic and toxic than trivalent chromium compounds (Polti et al., 2014).

Many techniques are used to reduce the Cr(VI) concentration in the environment (Cheung and Gu, 2003, 2005, 2007), such as sedimentation, chemical precipitation, membrane separation, ion exchange, ultrafiltration, and adsorption. The bioavailability, reactivity, and mobility of contaminants are well controlled by adsorption (Zheng et al., 2013; Qian et al., 2015). Therefore, it is necessary to prepare a low-cost adsorbent with a high adsorption capacity (Deveci and Kar, 2013; Tzeng et al., 2015). Carbon-rich biochar is pyrolyzed from various biomass feedstocks (Ahmad et al., 2012). Its application as an alternative adsorbent in recent years has attracted attention because it can remove different kinds of contaminants, including nutrients, heavy metals, and pharmaceuticals, from aqueous solutions (Inyang et al., 2012; Zhou et al., 2013). Many studies show that heavy metals can be immobilized by biochar and that the properties and structure of biochar play important roles in this process (Qian et al., 2015; Sun et al., 2014; Inyang et al., 2012). The performance of biochar is based on

* Corresponding author. College of environment and chemical engineering, Shanghai University, No.99, Shangda Road, Baoshan District, 200444, Shanghai, China.

E-mail address: lx999@shu.edu.cn (X. Liu).

characteristics such as pore size, specific surface area, surface functional groups, and pH, which depend on the pyrolysis temperature (Wang et al., 2013). In addition, the immobilization of heavy metals may be affected by the coexistence of other elements (Qian et al., 2015).

Much research has studied the effects of various types of biochar on the immobilization of a variety of heavy metals. Biochar made from the oily seeds of *Pistacia terebinthus* L., natural zeolite biochar, and blends of raw material with alumina biochar were used as low-cost adsorbents for the removal of chromium ions (Deveci and Kar, 2013). The adsorption characteristics of As(III)/As(V) ions and the effects of coexisting Cr(VI) on arsenic adsorption on coal-based activated carbon were studied (Gong et al., 2015). The incorporation of rice straw biochar into soil significantly increased the adsorption of Pb(II) by the soil (Jiang et al., 2012). Bamboo, sugarcane bagasse, hickory wood, and peanut hull were used to produce biochar. Almost all of these chitosan-modified biochars showed enhanced removal of three metals (Pb^{2+} , Cu^{2+} , and Cd^{2+}) compared to the unmodified biochars (Zhou et al., 2013). In addition, the adsorption of organic compounds by biochar has gained attention (Ahmad et al., 2014; Isah et al., 2015; Mohammed et al., 2015; Zheng et al., 2013). Previous research is useful for producing designer biochar that can reduce the toxicity of a specific heavy metal or the bioavailability of organic contaminants.

Above all, there are large numbers of published data involving heavy metal adsorption or organics adsorption solely. In fact, most wastewater often contains both heavy metals and organic pollutants, and therefore, it is necessary to investigate the influence of coexisting of organic pollutant on heavy metals adsorption. Pyrene was studied as a representative because it is among the commonly found hydrophobic organic contaminants (HOCs) in contaminated sites in the environment. In addition, its sorption has been widely characterized in previous studies (Zielinska and Oleszczuk, 2015; Chen et al., 2008; Zhang et al., 2014). Pineapple waste biomass was chosen as the raw material to produce biochar (pineapple-peel-derived biochar = PABC). Previous literature has reported on the characterization of biochar from pineapple for dye removal (Mahamad et al., 2015) and for improving pyrene bioremediation (Wang et al., 2015). However, little data is available on the effects of organic compounds on heavy metal sorption by biochar (Zhang et al., 2015).

The aim of this study was (1) to examine the effects of pyrolytic temperatures on the resulting biochar's physicochemical properties and on Cr(VI) sorption to PABC and (2) to investigate the influence of pyrene coexisting in aqueous solution with the biochar on Cr(VI) sorption. This work will provide an understanding of Cr(VI) adsorption on PABC and provide a reference for Cr(VI) removal by biochar in wastewater or Cr(VI) immobilization in soils amended with biochar.

2. Materials and methods

2.1. Characterization and preparation of PABC

Biochars were produced at various pyrolysis temperatures using pineapple peel. Pineapple peel was obtained from a fruit store at the campus of Wenzhou University, Wenzhou, China. Samples were washed several times with tap water, air-dried for one day, and oven-dried overnight at 70–80 °C. They were then easily ground and passed through a 100-mesh sieve (Chen et al., 2008). The powdered pineapple peel tightly filled a ceramic pot with a fitted lid to ensure oxygen-poor conditions. It was heated at various temperatures (350 °C, 500 °C, and 750 °C) in a muffle oven for 2 h with a heating rate of 5 °C min⁻¹. The charred solids were allowed to cool to room temperature and then immersed in 0.1 M HCl

solution overnight. Pumping filtration and repeated washing with distilled water was necessary to obtain a neutral filtrate prior to oven-drying the residue overnight at 50–60 °C. After cooling, the solids were passed through a 100-mesh sieve to gain the final biochar samples. The PABC samples were named B350, B500, and B700. The numbers represent the pyrolysis temperatures (Tytlak et al., 2015; Qian et al., 2015).

The surface area of the biochar was determined using an accelerated surface area and porosimetry system (ASAP, 2020 HD88, Micromeritics Instrument Corp., Norcross, GA, United States) with nitrogen adsorption at 77 K, and using the Brunauer-Emmett-Teller (BET) model, while micropore volume was determined from *t*-plot analysis. Fourier transform infrared spectroscopy (FTIR) was used to characterize the surface functional groups on the PABC. The spectra of samples were determined from wave numbers of 400–4000 cm⁻¹ by the KBr method on a FTIR spectrometer (TENSOR 27, Bruker Optics Inc., Germany), from the average of 64 scans at 4.0 cm⁻¹ resolution. Surface structure was measured using a scanning electron microscope (JSM-6700F, JEOL Ltd., Japan).

2.2. Batch sorption experiment

K₂Cr₂O₇ powder (guaranteed reagent, Sinopharm Chemical Reagent Co., Ltd., Shanghai, China) was dissolved in 0.1 mol L⁻¹ CaCl₂ as a background electrolyte to prepare the stock solution of Cr(VI) (500 mg L⁻¹). The adsorption experiment was conducted in 50 mL Erlenmeyer flasks. The initial hexavalent chromium concentration in the solution ranged from 10 to 100 mg L⁻¹. Then, 0.2 g biochar and 20 mL Cr(VI) solution with an initial pH of 4 were mixed into the flasks. All the flasks were sealed with silicon caps and then shaken at 120 rpm in a reciprocating shaker for 24 h to reach equilibrium, based on a preliminary study. After 24 h, a 0.45 µm Millipore filter was used to filter the solution. Finally, the standard colorimetric method with 1, 5-diphenylcarbazide was used to determine the hexavalent chromium concentration in the filtrate. In addition to the adsorption isotherm and kinetics, the influence of pH and of coexisting pyrene was investigated in several series of similar batch experiments, using the PABC pyrolyzed at 500 °C for 2 h.

2.3. Quality control and data analysis

The experiments were performed in triplicate at each temperature, including appropriate blanks and benchmarks. NaN₃ was added into the Cr(VI) solution containing pyrene to avoid microbial degradation. The adsorption of Cr(VI) was calculated using the loss from the initial solution after equilibrium, with respect to the values in the controls. We used a first-order kinetics equation and a second-order kinetics equation to investigate the kinetics of Cr(VI) adsorption onto PABC. The experimental data were fitted to Freundlich and Langmuir models.

3. Results and discussion

3.1. Biochar characterization

Table 1 shows the main characterization of PABC. The pyrolytic temperature significantly affected biochar production, with the yield dropping from 33.6% to 23.6% as temperature increased from 350 °C to 750 °C. This result supports a previous report that biochar yield significantly decreased from 72.5% at 300 °C to 52.9% at 700 °C (Khanmohammadi et al., 2015) and a report that biochar yield dropped from 77% to 23% as temperature increased from 250 °C to 600 °C (Ding et al., 2014). Another relevant study is Claoston et al. (2014).

Table 1
Characterization of the tested biochars.

| Sample | Yield (%) | Ash (%) | S_{BET} ($\text{m}^2 \text{g}^{-1}$) | Pore width (nm) | Pore volume ($\text{cm}^3 \cdot \text{g}^{-1}$) |
|--------|-----------|---------|---|-----------------|---|
| B350 | 33.6 | 3.8 | 0.7595 | 8.1 | 0.0017 |
| B500 | 27.8 | 3.6 | 2.157 | 5.7 | 0.0027 |
| B750 | 23.6 | 5.1 | 323.8 | 2.2 | 0.14 |

The surface area (S_{BET}) of the tested biochar increased with increasing pyrolytic temperature: B350 ($0.76 \text{ m}^2 \text{g}^{-1}$), B500 ($2.16 \text{ m}^2 \text{g}^{-1}$), and B750 ($323.80 \text{ m}^2 \text{g}^{-1}$; see Table 1). The decomposition of organic substances and the formation of micropores in the biochar at high temperatures may be the reasons for the increase in surface area (Ding et al., 2014); increasing pyrolytic temperature induced the development of a porous structure in the biochar, resulting in the higher internal surface area (Bonelli et al., 2007). Pore width declined with increased pyrolytic temperature. It is inferred that the relatively large pores were reduced to tiny pores (Table 1).

Scanning electron microscopy (SEM) images showed the surface characteristics of the PABC produced at the different temperatures and confirmed their porous structures (Fig. 1). As the temperature increased, the porous structure became more obvious. This result agrees with the data for S_{BET} (Table 1). The surfaces of B500 and B750 were clean, suggesting that the inorganic matter was swept away during washing. The literature indicates that biochar created at high temperature is more stable. Easily oxidizable organic matter, which can be retained in the biochar products, plays a significant role in the formation of the microporous structure of biochar (Qian et al., 2015).

The FTIR spectra of PABC created with various pyrolysis temperatures are illustrated in Fig. 2. The FTIR spectra of B500 before and after Cr(VI) sorption were used to detect changes in the vibration frequencies of the functional groups. C=C stretching caused the symmetric sorption band at 2310 cm^{-1} . The peak at 1099 cm^{-1} could be attributed to C–O groups. The peak observed at 1391 cm^{-1} corresponded to symmetrical C–H vibrations (Gomez-Serrano et al., 1996). Compared with B500 and B750, B350 had fewer peaks; the peak at 1535 cm^{-1} (C=O) was reduced, while the peak at 1099 cm^{-1} (C–O) disappeared. This result indicated that fewer chemical groups were present on the surface of the low temperature PABC than on the surface of the high temperature PABCs. This may explain the greater sorption capacity seen with increasing pyrolytic temperature. No significant changes in the functional groups of the biochar surface were observed before and after adsorption, demonstrating the slight contribution of organic matter and surface functional groups to chromium adsorption (Chen et al., 2015).

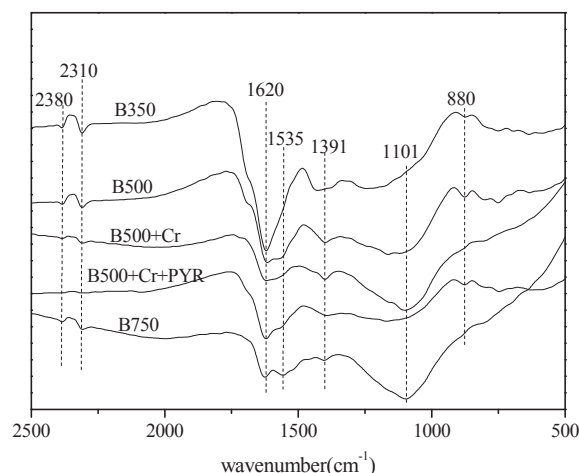


Fig. 2. FTIR spectra of PABCs used in the study. B500 indicates the B500 PABC sample before Cr(VI) sorption (B500) and after Cr(VI) sorption (B500 + Cr, B500 + Cr + PYR). In the experiment, 0.2 g biochar was shaken with 10 mg L^{-1} Cr(VI) (B500 + Cr) or with 10 mg L^{-1} Cr(VI) coexisting with 1 mg L^{-1} pyrene (B500 + Cr + PYR) for 24 h.

3.2. Adsorption kinetics of Cr(VI)

As shown in Fig. 3, Cr(VI) sorption on PABC has relatively slow kinetics. Equilibrium was achieved after 12 h for B750, 18 h for B350, and 24 h for B500. In most cases in the literature, more time is needed to reach the equilibrium of Cr(VI) adsorption onto the surface of biochar: more than 24 h (Zhang et al., 2013), approximately 80 h (Han et al., 2016), and even up to 96 h (Agrafioti et al., 2014). The main adsorption mechanism is the reduction of hexavalent chromium to trivalent chromium in the form of the aqueous complex $[\text{Cr}(\text{H}_2\text{O})_5]^{3+}$, which is adsorbed onto the surface of the biochar (Dobrowolski and Otto, 2010). The value of S_{BET} affected the speed of reaching equilibrium. B500 and B350 have lower specific surface areas than B750: $2.16 \text{ m}^2 \text{g}^{-1}$, $0.76 \text{ m}^2 \text{g}^{-1}$, and $323.80 \text{ m}^2 \text{g}^{-1}$, respectively.

We calculated the relevant kinetic parameters of the adsorption systems (Table 2) and plotted them in Fig. 4. The results indicate

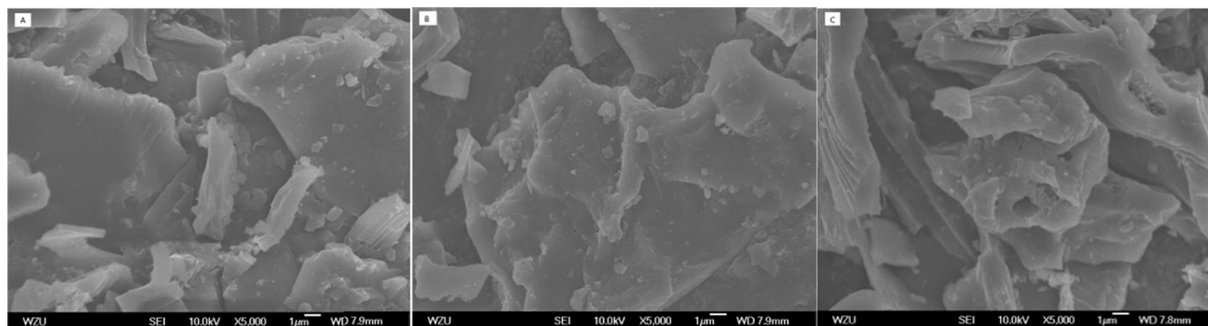


Fig. 1. SEM images of the PABC created at pyrolytic temperatures of (a) 350 °C, (b) 500 °C, and (c) 750 °C.

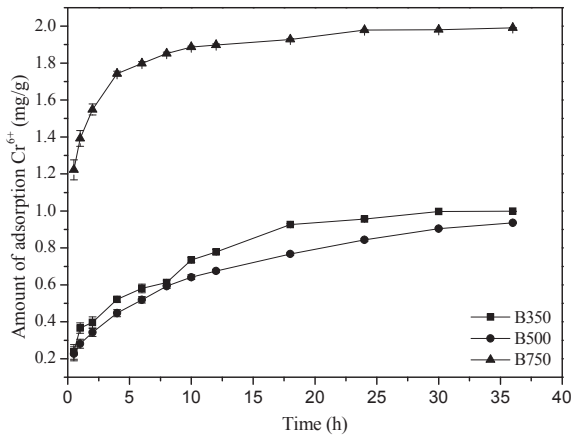


Fig. 3. Adsorption kinetics of Cr(VI) ions onto biochars; $m = 0.2$ g, $V = 20$ mL, $C_{Cr(VI)} = 10$ mg L⁻¹, pH = 2, and $T = 30$ °C.

Table 2

Parameters of pseudo-first-order and pseudo-second-order kinetic models for Cr(VI) adsorption onto biochars.

| Biochar | Kinetic model | | | | | |
|---------|--------------------|-------|----------|---------------------|-------|----------|
| | Pseudo-first-order | | | Pseudo-second-order | | |
| | k_1 | R^2 | Q_{eq} | k_2 | R^2 | Q_{eq} |
| B350 | 0.0040 | 0.872 | — | 0.0038 | 0.986 | 1.103 |
| B500 | 0.0039 | 0.612 | — | 0.0037 | 0.984 | 1.013 |
| B750 | 0.0036 | 0.834 | — | 0.0135 | 0.999 | 2.019 |

Q_{eq} is the amount adsorbed (mg·g⁻¹) at equilibrium, k_1 (min⁻¹) and k_2 (g·mg⁻¹·min⁻¹) are the rate constants of the pseudo-first-order equation and pseudo-second-order equation, respectively, and R is the regression coefficient.

that the first-order kinetics equation is a worse fit than the second-order kinetics equation; the correlation coefficients of B750 were 0.834 for first-order kinetics and 0.999 for second-order kinetics. Similar results were found in other studies focusing on Cr(VI) adsorption (Zhang et al., 2013; Aliabadi et al., 2012). Chemical sorption (chemisorption) can explain this phenomenon.

3.3. Sorption capacity of Cr(VI)

As shown in Table 3, Cr(VI) sorption on PABC fits better with the

Langmuir model (correlation coefficients $R^2 = 0.988$ – 0.992) than with the Freundlich equation (correlation coefficients $R^2 = 0.871$ – 0.953) at all pyrolysis conditions. The maximum sorption capacities were 2.49, 2.36, and 7.44 mg g⁻¹ for B350, B500, and B750, respectively. Previous studies have reported Cr(VI) adsorption by various biochars. For instance, the adsorption capacities of Cr(VI) by biochars derived from the seeds of *P. terebinthus* L., from blends of raw material with alumina, and from natural zeolite were 3.53 mg g⁻¹, 3.97 mg g⁻¹, and 6.08 mg g⁻¹, respectively (Deveci and Kar, 2013). Those of wheat straw biochar and wicker biochar were 24.6 and 23.6 mg g⁻¹, respectively (Tytlak et al., 2015), while that of oak bark biochar was 4.09 mg g⁻¹ (Mohan et al., 2011). Peanut hull biochar showed a capacity 1 to 2 orders of magnitude lower (below 10 mg g⁻¹) than magnetic biochar (Han et al., 2016). The performance of PABC in this study is similar to the performances of the other biochars reported by researchers. The n value indicating sorption intensity (Table 3) declines from B350 to B750, which can be explained by the smaller adsorption capacities for B350 and the greater energetic heterogeneity of B750.

As presented in Fig. 5, B750 has a greater adsorption capacity than B500 and B350. This is due to it having the largest BET surface area (323.80 m² g⁻¹) and may be partially correlated with its higher pore volume value (0.14 cm³/g). Tytlak et al. (2015) considered that Cr(VI) is adsorbed onto the PABC surface in the form of [Cr(H₂O)₅]³⁺. It is more difficult for chromium ions to pass through the pores of B350 and B500 than those of B750 because of the vast difference in the pore volumes. Thus, pore volume has an obvious effect on the adsorption process.

Table 3

Langmuir and Freundlich constants and correlation coefficients.

| Biochar | Langmuir | | | Freundlich | | |
|---------|----------|-------|-------|------------|------|-------|
| | b | Q_m | R^2 | K | n | R^2 |
| B350 | 0.067 | 2.49 | 0.992 | 0.113 | 0.49 | 0.953 |
| B500 | 0.191 | 2.36 | 0.991 | 0.255 | 0.34 | 0.871 |
| B750 | 0.360 | 7.44 | 0.988 | 0.375 | 0.26 | 0.936 |

Q_m is the maximum sorption capacity (mg·g⁻¹), b is the Langmuir constant (the quasi-Gaussian energetic heterogeneity of the adsorption system), R is the regression coefficient, K and n are empirical constants indicative of sorption capacity and sorption intensity, respectively.

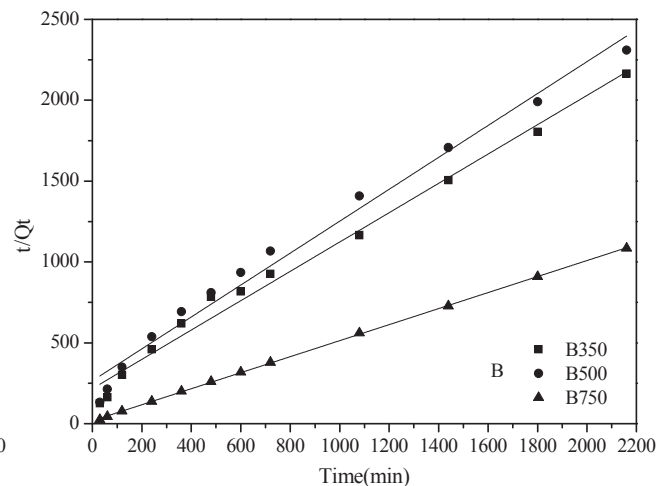
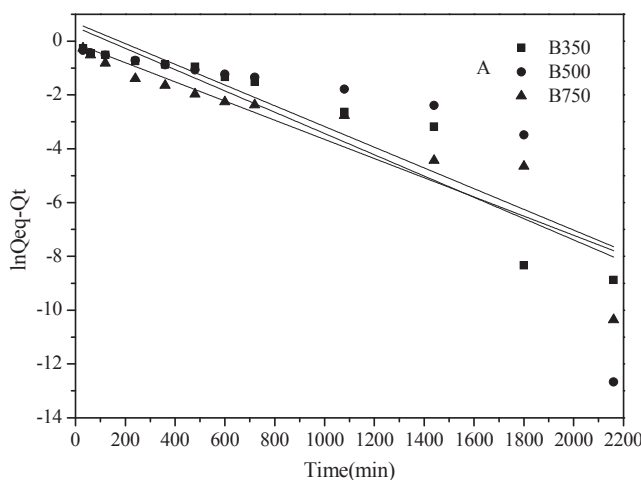


Fig. 4. The kinetic fitting plots of the pseudo-first-order equation (A) and pseudo-second-order equation (B) for the biochars. Q_t is the amount adsorbed (mg·g⁻¹) at time t , and Q_{eq} is the amount adsorbed (mg·g⁻¹) at equilibrium.

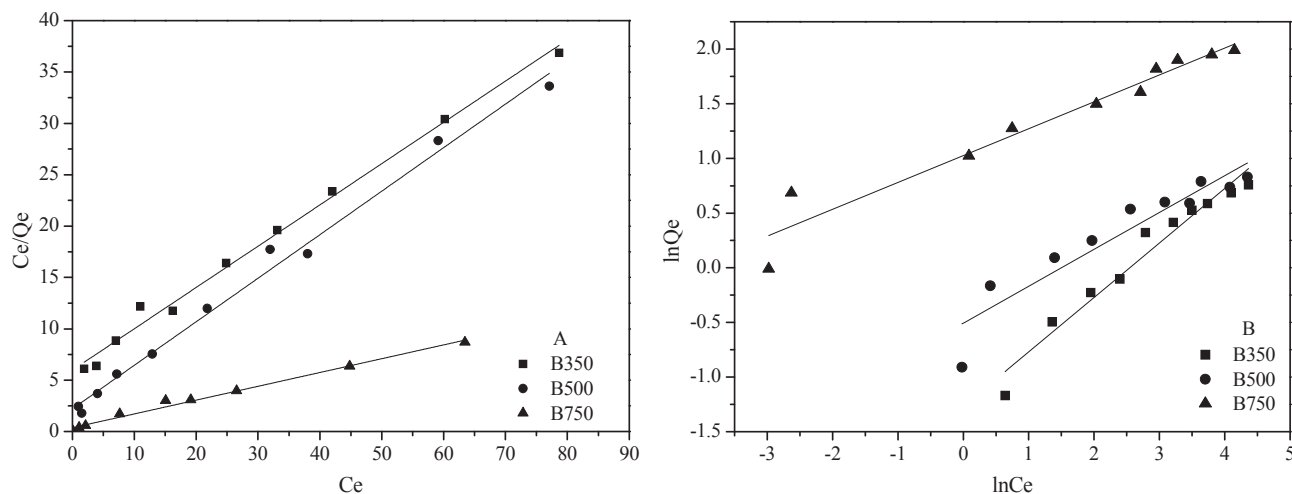


Fig. 5. Langmuir (A) and Freundlich (B) isotherms for Cr(VI) adsorption onto biochars.

3.4. Influence of pH on the adsorption of Cr(VI)

As illustrated in Fig. 6, we found that the greatest Cr(VI) sorption occurred at pH 2.0, which was approximately the zero charge potential ($pH_{zpc} = 1.5$) of PABC measured using the pH drift method (Sun et al., 2014). At this pH_{zpc} , no net electrical charge was present on the surface of the PABC, and the surface functional groups were almost neutral. The highest removal rate was greater than 95% and was reached when the initial concentration of Cr(VI) was 10 mg L^{-1} at pH 2.0. Previous studies showed the removal percentage of chromium on biochar derived from various biomasses: less than 80% for both oak wood and oak bark (Mohan et al., 2011), less than 40% for the seeds of *P. terebinthus* L. (Deveci and Kar, 2013), and less than 20% for municipal sewage sludge (Chen et al., 2015). All the optimal adsorption capacities were obtained at pH 2.0, including those found by Tytlak et al. (2015). The results of this study were consistent with previous studies.

3.5. Effect of pyrene on sorption of Cr(VI)

Fig. 7 illustrates that coexisting pyrene had an inhibition on the Cr(VI) sorption capacity although they may have the different adsorption mechanisms: cation exchange is one of the main

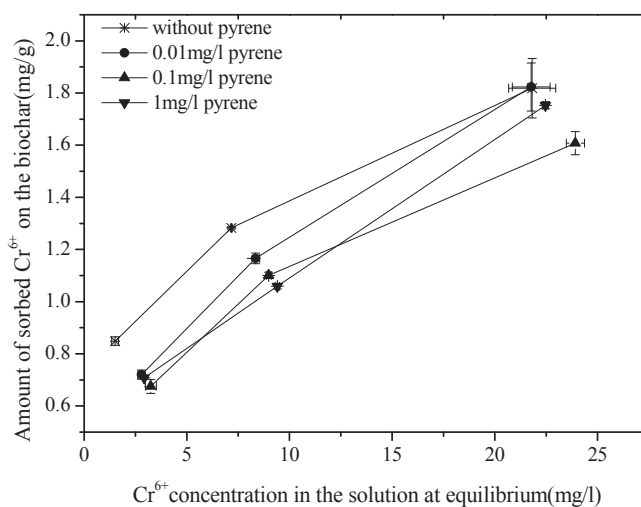


Fig. 7. Cr(VI) sorption influenced by coexisting pyrene.

adsorptive routes of Cr(VI), whereas distribution is dominant for pyrene. The sorption of pyrene primarily occurred in the

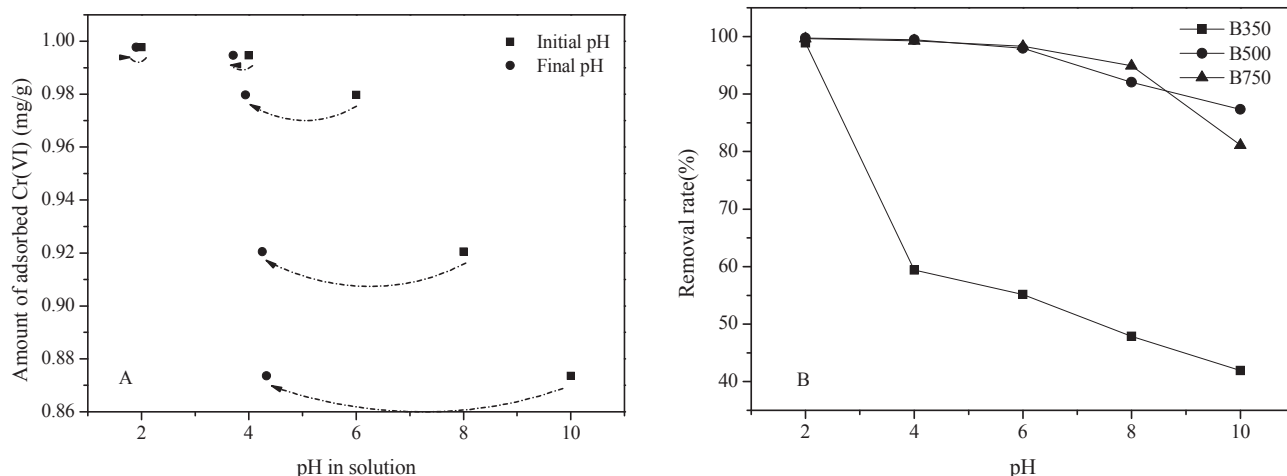


Fig. 6. Cr(VI) sorption influenced by solution pH. (A) shows Cr(VI) sorption on B500; (B) shows the removal rate of Cr(VI) from solution by the different biochars.

mesoporous regions of PABC as a result of the formation of successive adsorption layers, until the pores' volume was completely filled. The presence of additional hydrophobic and highly aromatic sorbents was found to create more favorable conditions for pyrene sorption (Zielinska and Oleszczuk, 2015). Therefore, when PABC is applied to contaminated soil with multiple pollutants, Cr(VI) removal may be influenced. In future studies, a sequential remediation process should be established, and the heavy metals and organic contaminants should be sequentially recovered or degraded, respectively (Zhang et al., 2015).

4. Conclusions

The effect of the pyrolytic temperature on the properties and adsorptive behavior of PABC was studied. The yield, pore properties, and surface functional groups changed with increasing pyrolytic temperature. However, no significant changes in the biochar surface functional groups were observed before and after the hexavalent chromium adsorption.

Cr(VI) sorption depends on pH; the optimum value is pH 2.0. The highest removal rate is greater than 95% when the initial concentration of Cr(VI) is 10 mg L⁻¹. The results indicate that Cr(VI) adsorption can be simulated with reasonable accuracy using the Langmuir model. The greatest Cr(VI) adsorption occurs on biochar pyrolyzed at 750 °C, which gives a maximum adsorption capacity of 7.44 mg g⁻¹. This biochar requires 18 h to approach the adsorption equilibrium, and its adsorption kinetics fit well with the second-order kinetic equation. It was also found that an alkaline pH in solution can intensively suppress Cr(VI) adsorption. When Cr(VI) and pyrene coexist in the matrix, pyrene can inhibit Cr(VI) adsorption, but the reduction is not proportional to the pyrene concentration. Still, competition of pyrene for the PABC sorption sites needs to be considered, as this may greatly limit the application of PABC to the removal of Cr(VI) under certain conditions, in particular when considerable levels of pyrene are present. On the other hand, it is necessary to research the influence of Cr(VI) and other main ions, such as Fe³⁺ and other hard ions, on pyrene sorption. The desorption behavior and potential degradation of PABC-immobilized pyrene should be further studied.

Acknowledgments

The work was funded by the National Natural Science Foundation of China (No. 41373097) and Program for Innovative Research Team in University (No.IRT13078).

References

- Agrafioti, E., Kalderis, D., Diamadopoulos, E., 2014. Arsenic and chromium removal from water using biochars derived from rice husk, organic solid wastes and sewage sludge. *J. Eviron. Manage.* 133, 309–314.
- Ahmad, M., Rajapaksha, A.U., Lim, J.E., Zhang, M., Bolan, N., Mohan, D., Vithanage, M., Lee, S.S., Ok, Y.S., 2014. Biochar as a sorbent for contaminant management in soil and water: a review. *Chemosphere* 99, 19–33.
- Ahmad, M., Lee, S.S., Yang, J.E., Ro, H.M., Lee, Y.H., Ok, Y.S., 2012. Effects of soil dilution and amendments (mussel shell, cow bone, and biochar) on Pb availability and phytotoxicity in military shooting range soil. *Ecotox. Environ. Safe* 79, 225–231.
- Aliabadi, M., Khazaei, I., Fakhræ, H., Mousavian, M.T.H., 2012. Hexavalent chromium removal from aqueous solutions by using low-cost biological wastes: equilibrium and kinetic studies. *Int. J. Environ. Sci. Te* 9, 319–326.
- Bonelli, P.R., Buonomo, E.L., Cukierman, A.L., 2007. Pyrolysis of sugarcane bagasse and co-pyrolysis with an argentinean subbituminous coal. *Energy Sour. Part A* 29, 731–740.
- Chen, B.L., Zhou, D.D., Zhu, L.Z., 2008. Transitional adsorption and partition of nonpolar and polar aromatic contaminants by biochars of pine needles with different pyrolytic temperatures. *Environ. Sci. Technol.* 42, 5137–5143.
- Chen, T., Zhou, Z., Xu, S., Wang, H., Lu, W., 2015. Adsorption behavior comparison of trivalent and hexavalent chromium on biochar derived from municipal sludge. *Bioresour. Technol.* 190, 388–394.
- Cheung, K.H., Gu, J.D., 2003. Reduction of chromate (CrO₄²⁻) by an enrichment consortium and an isolate of marine sulfate-reducing bacteria. *Chemosphere* 52, 1523–1529.
- Cheung, K.H., Gu, J.D., 2005. Chromate reduction by a *Bacillus magnetarum* TKW3 isolated from marine sediments. *World J. Microb. Biot.* 21, 213–219.
- Cheung, K.H., Gu, J.D., 2007. Mechanism of hexavalent chromium detoxification by microorganisms and bioremediation application potential: a review. *Int. Biodeter. Biodegr* 59, 8–15.
- Claoston, N., Samsuri, A.W., Husni, M.H.A., Amran, M.S.M., 2014. Effects of pyrolysis temperature on the physicochemical properties of empty fruit bunch and rice husk biochars. *Waste Manage. Res.* 4, 331–339.
- Deveci, H., Kar, Y., 2013. Adsorption of hexavalent chromium from aqueous solutions by bio-chars obtained during biomass pyrolysis. *J. Ind. Eng. Chem.* 19, 190–196.
- Ding, W., Dong, X., Ime, I.M., Gao, B., Ma, L.Q., 2014. Pyrolytic temperatures impact lead sorption mechanisms by bagasse biochars. *Chemosphere* 105, 68–74.
- Dobrowolski, R., Otto, M., 2010. Study of chromium(VI) adsorption onto modified activated carbons with respect to analytical application. *Adsorption* 16, 279–286.
- Gomez-Serrano, V., Pastor-Villegas, J., Perez-Florindo, A., Duran-Valle, C., Valenzuela-Calahorra, C., 1996. FT-IR study of rockrose and of char and activated carbon. *J. Anal. Appl. Pyro* 36, 71–80.
- Gong, X.J., Li, W.G., Zhang, D.Y., Fan, W.B., Zhang, X.R., 2015. Adsorption of arsenic from micro-polluted water by an innovative coal-based mesoporous activated carbon in the presence of co-existing ions. *Int. Biodeter. Biodegr* 102, 256–264.
- Han, Y.T., Cao, X., Ouyang, X., Sohi, S.P., Chen, J.W., 2016. Adsorption kinetics of magnetic biochar derived from peanut hull on removal of Cr (VI) from aqueous solution: effects of production conditions and particle size. *Chemosphere* 145, 336–341.
- Hsu, N.H., Wang, S.L., Lin, Y.C., Sheng, G.D., Lee, J.F., 2009. Reduction of Cr(VI) by crop-residue-derived black carbon. *Environ. Sci. Technol.* 43, 8801–8806.
- Inyang, M., Gao, B., Yao, Y., Xue, Y., Zimmerman, A.R., Pullammanappallil, P., Cao, X., 2012. Removal of heavy metals from aqueous solution by biochars derived from anaerobically digested biomass. *Bioresour. Technol.* 110, 50–56.
- Isah, U., Abdulraheem, G., Sala, S., Muhammad, S., Abdullahi, M., 2015. Kinetics, equilibrium and thermodynamics studies of CI reactive blue 19 dye adsorption on coconut shell based activated carbon. *Int. Biodeter. Biodegr* 102, 265–273.
- Jiang, J., Xu, R.K., Jiang, T.Y., Li, Z., 2012. Immobilization of Cu(II), Pb(II) and Cd(II) by the addition of rice straw derived biochar to a simulated polluted Ultisol. *J. Hazard. Mater* 229–230, 145–150.
- Khanmohammadi, Z., Afyuni, M., Mosaddeghi, M.R., 2015. Effect of pyrolysis temperature on chemical and physical properties of sewage sludge biochar. *Waste Manage. Res.* 3, 275–283.
- Mahamad, M.N., Zaini, M.A.A., Zainul, A.Z., 2015. Preparation and characterization of activated carbon from pineapple waste biomass for dye removal. *Int. Biodeter. Biodegr* 102, 274–280.
- Mohammed, J., Nasri, N.S., Zaini, M.A.A., Hamza, U.D., Ani, F.N., 2015. Adsorption of benzene and toluene onto KOH activated coconut shell based carbon treated with NH₃. *Int. Biodeter. Biodegr* 102, 245–255.
- Mohan, Jr., D., Pittman, C.U., 2006. Activated carbons and low cost adsorbents for remediation of tri- and hexavalent chromium from water. *J. Hazard. Mater* 137, 762–811.
- Mohan, D., Rajput, S., Singh, V.K., Steele Jr., P.H., Pittman, C.U., 2011. Modeling and evaluation of chromium remediation from water using low cost bio-char, a green adsorbent. *J. Hazard. Mater* 188, 319–333.
- Pan, J.J., Jiang, J., Xu, R.K., 2014. Removal of Cr(VI) from aqueous solutions by Na₂SO₃/FeSO₄ combined with peanut straw biochar. *Chemosphere* 101, 71–76.
- Polti, M.A., Aparicio, J.D., Benimeli, C.S., Amoroso, M.J., 2014. Simultaneous bioremediation of Cr(VI) and lindane in soil by actinobacteria. *Int. Biodeter. Biodegr* 88, 48–55.
- Qian, L., Chen, M., Chen, B., 2015. Competitive adsorption of cadmium and aluminum onto fresh and oxidized biochars during aging processes. *J. Soil. Sediment.* 15, 1130–1138.
- Sun, J., Lian, F., Liu, Z., Zhu, L., Song, Z., 2014. Biochars derived from various crop straws: characterization and Cd(II) removal potential. *Ecotox. Environ. Safe* 106, 226–231.
- Tytlak, A., Oleszczuk, P., Dobrowolski, R., 2015. Sorption and desorption of Cr(VI) ions from water by biochars in different environmental conditions. *Environ. Sci. Pollut. R.* 22, 5985–5994.
- Tzeng, J.H., Weng, C.H., Huang, J.W., Lin, Y.H., Lai, C.W., Lin, Y.T., 2015. Spent tea leaves: a new non-conventional and low-cost biosorbent for ethylene removal. *Int. Biodeter. Biodegr* 104, 67–73.
- Wang, C.H., Gu, L.F., Liu, X.Y., Ge, S.M., Chen, T.R., Hu, X.X., 2015. Removal of pyrene in simulated wetland by joint application of *Kyllinga brevifolia* Roth. and immobilized microbes. *Int. Biodeter. Biodegr.* <http://dx.doi.org/10.1016/j.ibiod.2015.11.008>.
- Wang, D.J., Zhang, W., Hao, X.Z., Zhou, D.M., 2013. Transport of biochar particles in saturated granular media: effects of pyrolysis temperature and particle size. *Environ. Sci. Technol.* 47, 821–828.
- Yu, X.Z., Gu, J.D., Huang, S.Z., 2007. Hexavalent chromium induced stress and metabolic responses in hybrid willows. *Ecotoxicology* 16, 299–309.
- Yu, X.Z., Gu, J.D., 2008. The role of EDTA in phytoextraction of hexavalent and trivalent chromium by two willow trees. *Ecotoxicology* 17, 143–152.
- Yu, X.Z., Gu, J.D., Xing, L.Q., 2008. Differences in uptake and translocation of hexavalent and trivalent chromium by two species of willows. *Ecotoxicology* 17,

- 747–755.
- Zhang, M., Shu, L., Shen, X., Guo, X., Tao, S., Xing, B., Wang, X., 2014. Characterization of nitrogen-rich biomaterial-derived biochars and their sorption for aromatic compounds. *Environ. Pollut.* 195, 84–90.
- Zhang, W., Mao, S., Chen, H., Huang, L., Qiu, R., 2013. Pb(II) and Cr(VI) sorption by biochars pyrolyzed from the municipal wastewater sludge under different heating conditions. *Bioresour. Technol.* 147, 545–552.
- Zhang, W., Zheng, J., Zheng, P., Qiu, R., 2015. Atrazine immobilization on sludge derived biochar and the interactive influence of coexisting Pb(II) or Cr(VI) ions. *Chemosphere* 134, 438–445.
- Zheng, H., Wang, Z., Zhao, J., Herbert, S., Xing, B., 2013. Sorption of antibiotic sulfamethoxazole varies with biochars produced at different temperatures. *Environ. Pollut.* 181, 60–67.
- Zhou, Y., Gao, B., Zimmerman, A.R., Fang, J., Sun, Y., Cao, X., 2013. Sorption of heavy metals on chitosan-modified biochars and its biological effects. *Chem. Eng. J.* 231, 512–518.
- Zielinska, A., Oleszczuk, P., 2015. Evaluation of sewage sludge and slow pyrolyzed sewage sludge-derived biochar for adsorption of phenanthrene and pyrene. *Bioresour. Technol.* 192, 618–626.